

Printing nanoparticles from the liquid and gas phases using nanoxerography

Chad R Barry, Michael G Steward, Nyein Z Lwin and Heiko O Jacobs¹

Department of Electrical and Computer Engineering, University of Minnesota, 200 Union Street SE, Minneapolis, MN 55455, USA

E-mail: hjacobs@ece.umn.edu

Received 24 March 2003, in final form 28 May 2003

Published 27 August 2003

Online at stacks.iop.org/Nano/14/1057

Abstract

This paper reports on the directed self-assembly of nanoparticles onto charged surface areas with a resolution of 200 nm from the liquid phase and 100 nm from the gas phase. The charged areas required for this type of nanoxerographic printing were fabricated using a parallel method that employs a flexible, electrically conductive, electrode to charge a thin-film electret. As electrodes, we used metal-coated polymeric stamps and 10 μm thick doped silicon wafers carrying a pattern in topography. Each electrode was brought in contact with a thin-film electret on an n-doped silicon substrate. The charge pattern was transferred into the thin-film electret by applying a voltage pulse between the conductive electrode and the silicon substrate. Areas as large as 1 cm^2 were patterned with charge with 100 nm scale resolution in 10 s. These charge patterns attract nanoparticles. A liquid-phase assembly process where electrostatic forces compete with disordering forces due to ultrasonication has been developed to assemble nanoparticles onto charged based receptors in 10 s from a liquid suspension. A gas-phase assembly process was developed that uses a transparent particle assembly module to direct particles towards the charged surface while monitoring the total charge of assembled particles. Nanoparticles were generated using a tube furnace by evaporation and condensation at the outlet. The electrostatically directed assembly of 10–100 nm sized metal (gold, silver) and 30 nm sized carbon particles was accomplished with a resolution 500–1000 times greater than the resolution of existing xerographic printers.

1. Introduction

Nanoparticles can provide a variety of functions and are considered as building blocks of future nanotechnological devices. Nanoparticles are typically created in the gas or liquid phase. The best known techniques include metal evaporation, laser ablation, solution vaporization, wire explosion, pyrolysis, colloidal and electrochemical synthesis and generation from plasmas. Nanoparticles are of current interest for electronic and optoelectronic device applications. Silicon nanoparticles generated by silane pyrolysis or electrochemical reaction of hydrogen fluoride with hydrogen peroxide are used for non-volatile memories [1], lasers [2] and biological

markers [3]. Evaporated gold [4], indium [5] and ion sputtered aluminium [6] nanoparticles are used for single-electron transistors, and electron beam evaporated gold and silver particles are used for plasmonic waveguides [7]. Novel devices, however, do not hold the only interest in nanoparticle generation. Nanoparticles also provide the foundation for the development of new materials and act as catalysts in nanowire synthesis [8].

The use of nanoparticles as building blocks, regardless of the application, requires new assembling strategies. The most actively studied approaches include (i) single-particle manipulation [9, 10], (ii) random particle deposition [1, 5, 6] and (iii) parallel particle assembly—based on self-assembly [11–29]. Single-particle manipulation and random particle deposition

¹ Author to whom any correspondence should be addressed.

are useful to fabricate and explore new device architectures. However, inherent disadvantages such as the lag in yield and speed will have to be overcome in the future to enable the manufacturing of nanotechnological devices. Fabrication strategies that rely on mechanisms of self-assembly can overcome these difficulties. We and others have begun to use self-assembly to assemble nanoparticles onto substrates. Current areas of investigation use geometrical templates [11, 12], copolymer scaffolds [13], protein recognition [14, 16], DNA hybridization [17–20], hydrophobicity/hydrophilicity [21, 22], magnetic interactions [23, 24] and electrostatic interactions [25–29].

Stimulated by the success of atomic force based charge patterning, Wright and Chetwynd suggested in 1998 [30] that high resolution charge patterns could be used as templates for self-assembly and as nucleation sites for molecules and small particles. Since then, several serial charge-patterning processes have been explored to enable the positioning of nanoparticles. Scanning probe based techniques for example have been developed by Jacobs and Stemmer and Mesquida and Stemmer to pattern charge in silicon dioxide [31] and Teflon-like thin films [32]. Serial techniques, however, remain slow—the fastest scanning probe based system needs 1.5 days to pattern an area of 1 cm² [33]. This experimental bottleneck led to the development of electric nanocontact printing to pattern charge in parallel [25], and subsequently nanoxerographic printing [26]. Electric nanocontact printing generates a charge pattern based on the same physical principles as used in scanning probes but forms multiple electric contacts of different sizes and shapes to transfer charge in a single step. With this method, we demonstrated patterning of charge with 100 nm scale resolution and transfer of 50 nm to 20 μ m sized particles including iron oxide, graphitized carbon, iron beads and Xerox toner [25, 26]. As a result, several research groups have begun investigating charge based printing. Krinke *et al* [34] assembled indium particles from the gas phase onto charged areas created by contact charging using a scanning stainless steel needle and a nickel plate; Mesquida *et al* [27, 35] demonstrated the assembly of silica beads and gold colloids from the liquid phase onto charged areas created by contact charging using a scanning probe and Fudouzi *et al* [29, 36] demonstrated the assembly of SiO₂ and TiO₂ particles from both the liquid and gas phases onto charged areas created by focused ion and electron beams. Our parallel nanoxerographic process [26] provides the ability to fabricate numerous charged samples in a reasonable amount of time. Consequently, fast screening for conditions that allow assembly becomes possible. As a result, we were able to demonstrate particle transfer from powder, gas and liquid phases [26]. Our technique has also been adopted by others. For example, Krinke *et al* [28] demonstrated the assembly of gold nanoparticles from an aerosol.

This paper reports on recent progress in nanoxerography. We discuss improved assembly techniques that outperform our previously reported methods [26]. We demonstrate charge patterning using flexible thin silicon electrodes and nanoxerographic printing from the liquid and gas phases. We describe an improved liquid-phase assembly strategy and report on a gas-phase particle assembly module that uses a global electrostatic field to direct nanoparticles towards a charged surface. Nanoxerographic printing is demonstrated

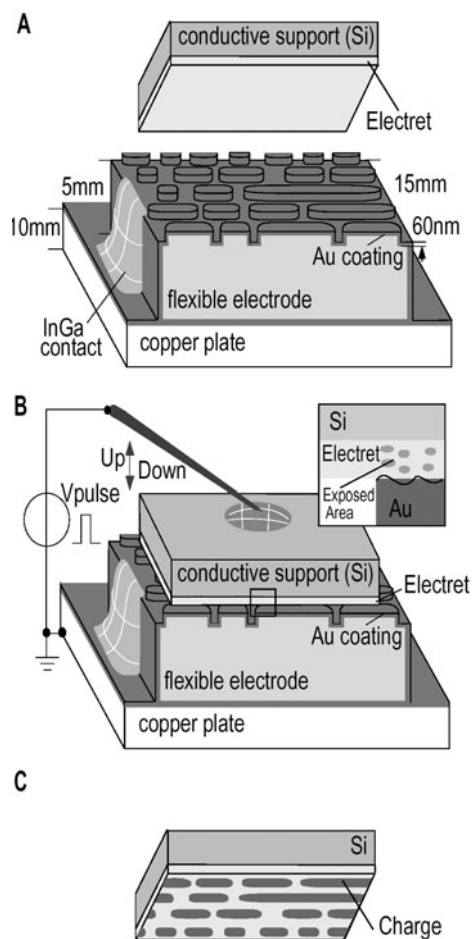


Figure 1. Principle of parallel charge patterning. (A) A silicon chip carrying a thin-film electret is placed on top of a flexible electrode on a copper plate. (B) A needle, attached to a micromanipulator, is brought into contact with the silicon chip. An external voltage is applied between the needle and the copper support to generate a pattern of charge in the electret material. (C) The silicon chip is removed with the electret carrying a charge pattern.

with a resolution of 200 nm from the liquid phase and 100 nm from the gas phase, which is 500–1000 times the resolution of traditional xerographic printers [37, 38].

2. Experimental details

The electric nanocontact printing process to generate charge patterns is illustrated in figure 1. A silicon chip coated with a thin-film electret is placed on top of a flexible conductive electrode carrying a pattern in bas relief. The flexibility of the electrode structure allows the formation of multiple electric contacts of different sizes and shapes between both surfaces. An external voltage pulse is applied between the flexible electrode and the rigid silicon chip to transfer charge into the thin-film electret.

In our experiments, we tested two different flexible electrodes to accomplish charge transfer. The first electrode prototype was made out of a 5 mm thick poly-(dimethylsiloxane) (PDMS) stamp, patterned in bas relief using procedures described before [39]. To make the stamp electrically conducting, we supported it on a copper plate and

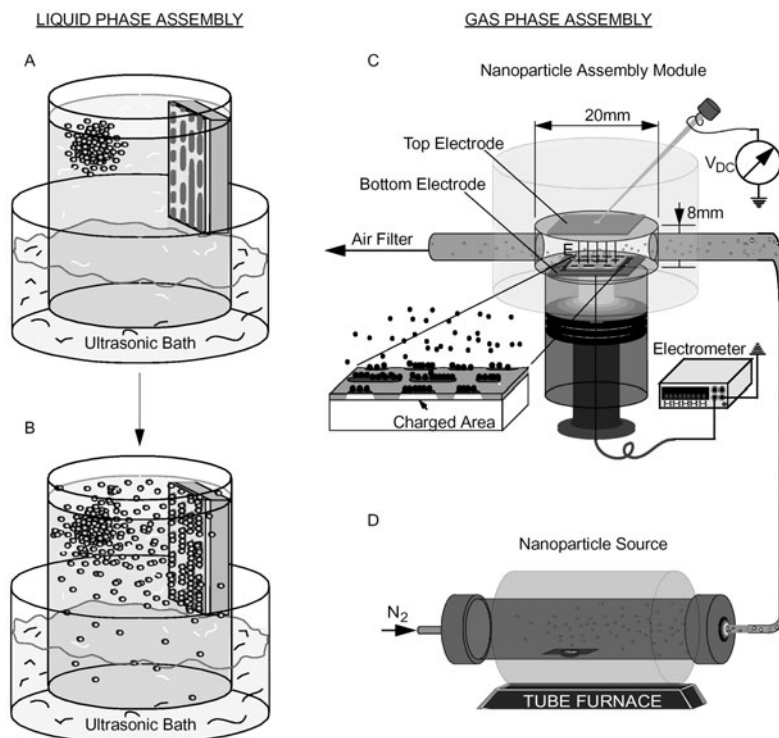


Figure 2. Principal of nanoxerographic printing from the liquid and gas phases. *Liquid phase.* (A) The chip carrying a charge pattern is immersed in the solvent under sonication. A $\sim 500 \mu\text{m}$ large aggregate of graphitized carbon nanoparticles is placed in the solvent. (B) The graphitized carbon nanoparticles disperse in the solvent and assemble on the charged areas of the chip. *Gas phase.* (C) The directed assembly of the nanoparticles occurs in the particle assembly module. An external potential, V_{DC} , applied to the top electrode directs incoming nanoparticles to the charged sample surface. The electrometer measures the number of assembled, charged particles during the assembly process. (D) A constant flow of nanoparticles is generated by evaporation of matter in the tube furnace, transport of the atoms to the outlet by the N_2 gas and condensation.

thermally evaporated a 60 nm thick gold film onto it. We applied InGa (a liquid metal alloy, Aldrich) to the sidewalls of the stamp to provide a good contact to the copper plate. The second electrode prototype was made from a 3 inch diameter, 10 μm thick, n-doped silicon wafer (Virginia Semiconductors). A pattern in topography, consisting of 450 nm wide and 200 nm deep silicon lines, was transferred into the silicon by phase-shift lithography [40] and etching in a 98% CF_6 , 2% O_2 plasma. The n-doped silicon is sufficiently conductive and does not require a metal coating. To provide an equal pressure distribution and uniform electric contact, we placed the non-patterned side of the thin silicon electrode on a gold-coated flat piece of PDMS on a copper plate.

As the electret, we tested two different dielectric materials, poly-(methylmethacrylate) (PMMA), a commercially available electret with good charge storage capabilities [41], and SiO_2 . For the PMMA electret, we used a 2% solution of 950 K PMMA in chlorobenzene (MicroChem Co.) and spin coating at 5000 rpm to form a thin film on a silicon wafer. We cleaned the wafer in a 1% solution of hydrofluoric acid to remove the native oxide prior to spin coating. The spin-coated wafer was baked in an oven at 90 $^\circ\text{C}$ for 1 h. For the SiO_2 electret, a 50 nm thick wet oxide was thermally grown in an oxygen furnace at 1100 $^\circ\text{C}$ for 30 min. Both electrets were formed on (100) n-doped silicon wafers with a resistivity of 3 $\Omega \text{ cm}$ that were cut into 0.5–1 cm^2 sized chips after processing. To form an electrical connection we spread liquid InGa on the backside of these chips. The chips were placed on the

flexible electrode by hand and contacted with a metallic needle attached to a micromanipulator.

To generate a pattern of trapped charge, we applied an external potential for 1–10 s. During the exposure, we monitored the current flow and adjusted the voltage (5–20 V) to get an exposure current of 0.1–1 mA. After exposure, we removed and characterized the charge patterns using Kelvin probe force microscopy (KFM) [42]. KFM involves the use of an atomic force microscope (AFM) probe to detect electrostatic forces. We developed a KFM procedure that enables us to measure the charge and surface potential distribution with 100 nm scale resolution [42, 43].

The nanoxerographic process to direct the assembly of nanoparticles is illustrated in figure 2. The liquid-phase assembly process depicted on the left uses sonication to disperse commercially available nanoparticles in a non-polar solvent such as perfluorodecalin and Fluorinert FC-77. Both solvents have a relative dielectric constant of 1.8 and work equally well. In the liquid phase, we tested iron beads, $< 2 \mu\text{m}$ in size, red iron oxide particles, $< 500 \text{ nm}$ in size, and graphitized carbon nanoparticles, 30 nm in size. The particles were obtained from PolyScience (Niles, IL) in the form of a powder. The red iron oxide and the graphitized carbon powder contained loosely bound aggregates of primary particles. To assemble the nanoparticles, we place the chip carrying a charge pattern into a vial that contains 1 ml of solvent that is being sonicated using an ultrasonic bath. Subsequently, we placed a large particle aggregate, $< 500 \mu\text{m}$ in size for red iron oxide and graphitized carbon, into the solvent. The sonication breaks

up the aggregate and small particles disperse and align on the charged surface areas within seconds. The dispersion becomes visible due to a slight colour change in the assembly solution. Immediately (~ 2 s) after the dispersion is recognized, the chip is removed and dried under nitrogen. The entire assembly process takes only 5–10 s. This process provided higher resolution and selectivity than assembly without sonication.

The gas-phase assembly process (C), (D) depicted on the right uses a particle assembly module to accomplish the directed assembly of nanoparticles. The module (C) consists of a cavity that holds the sample, two electrodes to generate a global electric field that directs incoming charged particles towards the sample surface and an electrometer to count the charge of the assembled particles. This module is attached to a tube furnace (D) that generates the nanoparticles by evaporation and condensation. The particle assembly module was constructed out of transparent PDMS. We chose a transparent material to allow visual inspection during the assembly process. Individual nanoparticles are difficult to visualize by optical means. However, a surface with micrometre sized areas that is covered with nanoparticles during the assembly process exhibits an optically visible diffraction pattern. PDMS can be moulded around readily available objects in successive steps to form the three-dimensional assembly module. In the first step, we formed the cavity by moulding PDMS around a 20 mm diameter and 8 mm tall disc that was removed after curing the PDMS at 60°C . In the second step, we formed a sample exchange unit by attaching a rigid polyethylene tube to the cavity using PDMS. The tube holds a retractable cylinder that carries the sample. To form a particle inlet and outlet we inserted a stainless steel tube 5 mm in diameter into each side of the PDMS shell.

To direct the assembly of incoming charged particles we integrated two electrodes into the transparent assembly module: a 2 cm long and 1 cm wide electrode located at the top of the cavity and a $1.5\text{ cm} \times 1\text{ cm}$ wide electrode underneath the sample. During operation, the electrodes are spaced by ~ 7 mm and we apply an external voltage of up to +1000 V to bring charged particles of one polarity into the proximity of the charged sample surface.

To monitor the number of particles that assembled onto the sample under different assembly conditions we implemented a Faraday cup in the assembly module. In our Faraday cup arrangement, the sample forms the cup electrode and is connected to ground with the electrometer (Keithley 6517A) in between. During assembly, image charges flow from the ground through the electrometer into the sample to the location of assembled, charged particles. As a result, the electrometer measures the charge of the assembled particles.

The particles were generated in a tube furnace [44]. The material to be evaporated was placed inside the quartz tube at the centre of the furnace. Pure nitrogen was the carrier gas that flows through the system during operation. The evaporation was carried out at 1100°C . A vapour containing atoms of the evaporated material forms within the furnace. The nitrogen carrier gas transports the atoms out of the furnace where they nucleate and condense into particles due to the change in temperature. The gas flow carries the nanoparticles into the particle assembly module through a 1 m long Tygon tube.

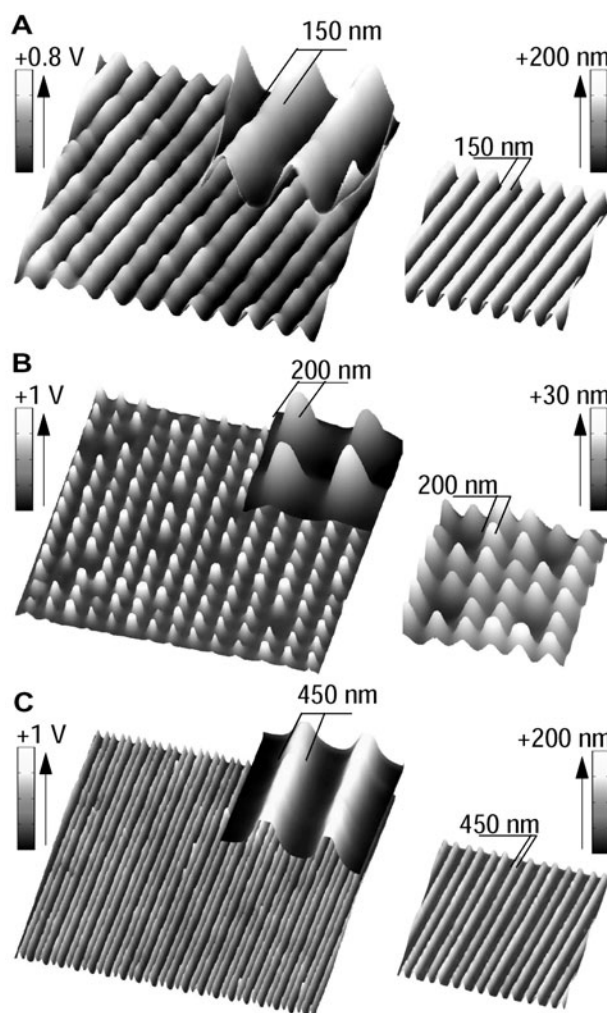


Figure 3. KFM images of patterns of positive charge (left) in PMMA and corresponding AFM images of the topography (right) of the electrode structures used to generate the charge patterns. (A) Surface potential image of 150 nm (FWHM) positively charged parallel lines generated using a stamp carrying <200 nm wide parallel lines. (B) Surface potential image of positively charged dots, 200 nm in diameter, that were generated using circular posts that were 30 nm high. (C) Surface potential image of 450 nm (FWHM) positively charged lines generated using a thin silicon electrode.

3. Results and discussion

Figure 3 illustrates three representative patterns of localized charge in PMMA that were recorded by KFM. A corresponding topographic AFM image of the electrode structure used to generate the pattern is displayed on the right-hand side of each KFM image. Figure 3(A) shows the surface potential for a surface patterned with 150 nm wide (FWHM) parallel lines. Figure 3(B) shows 200 nm sized dots. Each pattern was generated with a metal coated PDMS electrode that was fabricated from a Si mould defined by e-beam lithography. Figure 3(C) shows a surface potential image of 450 nm wide (FWHM) parallel lines. This pattern was generated with a thin silicon electrode. All charge patterns were written by exposing the PMMA film locally with a current density of 1 mA cm^{-2} for 10 s with the electrode positive. With the recorded surface potential distribution, it is possible to

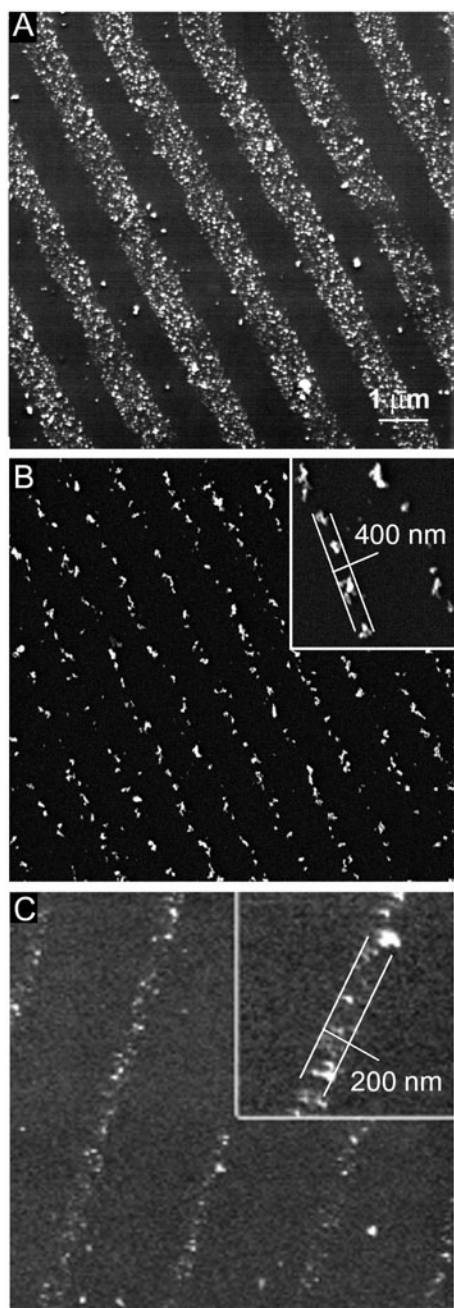


Figure 4. SEM images of graphitized carbon nanoparticles assembled from the liquid phase. (A) Assembly of particles on $1\ \mu\text{m}$ wide positively charged lines. (B), (C) Assembly of particles on areas patterned with $200\ \text{nm}$ wide lines; the cluster size determines the width of the assembled lines.

calculate a first order estimate of the trapped charge density. Trapped charge inside or on the surface of the PMMA film will attract mobile charge carriers that lie within the silicon substrate, resulting in the formation of a double layer. To derive a first estimate for the charge density we assume that this double layer is separated by a distinct distance d . The charge density σ can then be calculated with $\sigma = \epsilon \Delta V / d$, where ϵ is the permittivity, and ΔV is the voltage drop across the layer [45]. For $\epsilon = 8 \times 10^{-12}\ \text{C}\ (\text{V m})^{-1}$ (permittivity of PMMA), $\Delta V = 1\ \text{V}$ (measured potential change) and $d = 50\ \text{nm}$ (assumed intermediate distance between the

counter-charges), we obtain an estimate of the effective charge density of $\sigma_{\text{eff}} = 100$ elementary charges per surface area of $100\ \text{nm} \times 100\ \text{nm}$.

Figure 4 shows representative images of nanoxerographic printing of nanoparticles from the liquid phase. The images show patterns of graphitized carbon trapped at charged areas on PMMA. The patterns cover areas up to $5\ \text{mm} \times 5\ \text{mm}$ in size. The resolution is typically $400\ \text{nm}$ over large areas and $200\ \text{nm}$ over small areas. The resolution is currently limited due to the presence of primary particle clusters that are up to $400\ \text{nm}$ in size. The sonication is insufficient to break up these clusters. We noticed that the cluster size increased over time in the non-polar solvent; high resolution was only obtained using fresh suspensions. We have not yet determined the actual charge on these particles. In the presented results the different particles were trapped with positive charge patterns. However, we found that the same particles can be trapped with negative charge patterns as well. This phenomenon suggests that the assembly process is dominated by a real charge-induced dipole interaction; i.e. trapped charge in the thin-film electret induces a dipole on the particle causing an attractive net force between a polarizable particle and a charged surface area.

Figure 5 shows representative images of nanoxerographic printing of nanoparticles from the gas phase. The patterns cover areas up to $5\ \text{mm} \times 5\ \text{mm}$ in size. Figure 5(A) shows patterns of silver nanoparticles that assembled on the positively charged areas from the gas phase. The resolution achieved is $190\ \text{nm}$. Along with silver, we observed ordering of gold particles. Figures 5(B) and (C) show gold nanoparticles assembled onto negatively charged 500 and $200\ \text{nm}$ wide lines and rings. Figure 5(D) shows silver particles assembled on a substrate patterned with positive charge using the thin silicon electrode. Figure 5(E) shows a small area of silver nanoparticles assembled onto $100\ \text{nm}$ wide lines. The global electric field and the electrometer reading are two important parameters to control the assembly process, the particle polarity that assembles on the surface, the speed of the assembly and the coverage. Nanoparticles assembled well on positively charged areas (figures 5(A), (D) and (E)) by applying a negative potential to the top electrode, whereas for negatively charged areas (figures 5(B) and (C)) a positive potential was required. The polarity of the external potential also defined which majority, positively or negatively charged particles, assembled onto the sample. During the assembly of silver nanoparticles at a positive potential of $1\ \text{kV}$ and a flow rate of $1000\ \text{cm}^{-3}$, the charge on the sample, recorded by the electrometer, increased by $+4\ \text{nC}$ in $1\ \text{min}$, whereas at a negative bias of $-1\ \text{kV}$ the charge increased by $-4\ \text{nC}$. An increase in charge was also observed when no potential was applied. The charge rate in this case, however, was much slower than $4\ \text{nC min}^{-1}$. No increase in charge was observed without flow. This result can only be explained by the coexistence of positively and negatively charged particles that are transported through the system. This result is interesting because it is not obvious how the particles become charged in our system. One possible explanation is that the nanoparticles as well as the carrier gas are charged by thermal ionization [46] and natural radiation ionization. Both mechanisms are well known in aerosol systems. The global electric field also affected how fast the assembly took place: at $1\ \text{kV}$ the assembly

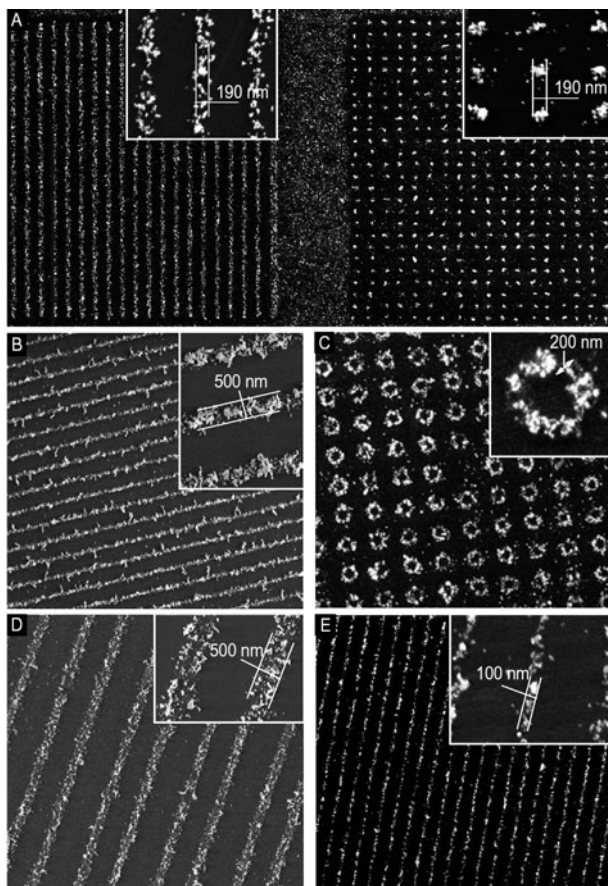


Figure 5. SEM images of different nanoparticle assemblies from the gas phase. (A) Image illustrates one section of a sample with trapped silver nanoparticles, patterned with 190 nm sized features. (B), (C) Gold nanoparticles assembled onto negatively charged 500 and 200 nm wide lines and rings. (D), (E) Silver nanoparticles assembled onto positively charged 500 and 100 nm wide lines. Image (D) was patterned using the thin silicon electrode. All other images were patterned with PDMS electrodes.

time to get good coverage was 1 min whereas at 100 V it took 10 min to get the same coverage. We also observed a clear proportionality between the electrometer reading and the coverage. Excellent coverage and high selectivity were obtained when 4 nC of charged silver particles accumulated on the sample, whereas at 10 nC the sample would be fully coated.

4. Conclusions

In conclusion, we have demonstrated nanoxerographic printing of different nanoparticles from the liquid and gas phases. Nanoxerography relies on a high resolution charge patterning technique, electric nanocontact printing, which is based on a flexible electrode structure that forms multiple electric contacts of different sizes and shapes to an electret surface. The resolution of this patterning technique is currently limited by the smallest possible feature size that we can fabricate on the electrode structure. For the PDMS based electrode structure this limit is approximately 100 nm. Smaller features tend to collapse. Higher resolution might be accomplished with the thin silicon based electrode prototype. Silicon is

capable of supporting ~ 10 nm sized features [47]. The first results of nanoxerographic printing using the thin silicon are very encouraging as it presents a possible route to sub-100 nm resolution. So far, there are many open questions on the charging process itself. For example, in our charging experiments we found that changing the exposure time and current has little effect on the amount of charge transferred. In several experiments, the surface potential remained the same whether the sample was exposed to a current of 100 μA for 2 s or to a current of 10 mA for 30 s. This result suggests that the maximum charge level might be achieved with even smaller exposure times and currents.

The best resolution obtained in nanoxerographic printing is between 100 and 200 nm, which is 500–1000 times the resolution of traditional xerographic printers [37, 38]. The improvement in resolution compared to our previously reported results [26] has become possible due to a new liquid-phase assembly procedure in which electrostatic forces compete with disordering forces, and due to a gas-phase particle assembly module in which charged particles are selected and directed towards the sample surface. The assembly module could, in principle, be attached to other gas-phase particle generation systems. The module allows the study of particle assembly as a function of the global external field and flow rate. The ability to monitor how many charged particles have assembled on the chip surface during the experiment has been very useful in optimizing this procedure. There are still many open questions that need to be addressed. For example, it is not clear what the ultimate resolution limit of patterned charge is and what experimental conditions are best to achieve particle assembly at charge surface areas. We expect that the assembly process depends on the actual charge on the particle, the electric polarizability of the particle, the thermal energy of the particle, the electric field strength at the substrate surface, the van der Waals interaction between the particles and substrate surface, the surrounding medium and the pressure. Nanoxerography, in summary, offers a very competitive strategy compared to other techniques. It can handle all kinds of material, is parallel and potentially could accomplish 10 nm scale resolution or better.

Acknowledgment

Financial support from the National Science Foundation (DMI-0217538, ECS-0229087 and IGERT) is gratefully acknowledged.

References

- [1] Ostraat M L, De Blauwe J W, Green M L, Bell L D, Brongersma M L, Casperson J, Flagan R C and Atwater H A 2001 *Appl. Phys. Lett.* **79** 433
- [2] Nayfeh M H, Rao S, Barry N, Therrien J, Belomoin G, Smith A and Chaieb S 2002 *Appl. Phys. Lett.* **80** 121
- [3] Belomoin G, Therrien J, Smith A, Rao S, Twesten R, Chaieb S, Nayfeh M H, Wagner L and Mitas L 2002 *Appl. Phys. Lett.* **80** 841
- [4] Thelander C, Magnusson M H, Deppert K, Samuelson L, Poulsen P R, Nygard J and Borggreen J 2001 *Appl. Phys. Lett.* **79** 2106
- [5] Junno T, Magnusson M H, Carlsson S-B, Deppert K, Malm J-O, Montelius L and Samuelson L 1999 *Microelectron. Eng.* **47** 179

- [6] Kim T W, Choo D C, Shim J H and Kang S O 2002 *Appl. Phys. Lett.* **80** 2168
- [7] Maier S A, Brongersma M L, Kik P G, Meltzer S, Requicha A A G and Atwater H A 2001 *Adv. Mater.* **13** 1501
- [8] Duan X, Huang Y, Agarwal R and Lieber C M 2003 *Nature* **421** 241
- [9] Baur C, Bugacov A, Koel B E, Madhukar A, Montoya N, Ramachandran T R, Requicha A A G, Resch R and Will P 1998 *Nanotechnology* **9** 360
- [10] Resch R, Bugacov A, Baur C, Koel B E, Madhukar A, Requicha A A G and Will P 1998 *Appl. Phys. A* **67** 265
- [11] Norris D J and Vlasov Y A 2001 *Adv. Mater.* **13** 371
- [12] Xia Y N, Gates B and Li Z Y 2001 *Adv. Mater.* **13** 409
- [13] Lopes W A and Jaeger H M 2001 *Nature* **414** 735
- [14] Janin J 1995 *Prog. Biophys. Mol. Biol.* **64** 2
- [15] Fudouzi H, Kobayashi M, Egashira M and Shinya N 1997 *Adv. Powder Technol.* **8** 251
- [16] Moore J T, Beale P D, Winningham T A and Douglas K 1997 *Appl. Phys. Lett.* **71** 1264
- [17] Niemeyer C M, Ceyhan B, Gao S, Chi L, Peschel S and Simon U 2001 *Colloid Polym. Sci.* **279** 68
- [18] Mirkin C A, Letsinger R L, Mucic R C and Storhoff J J 1996 *Nature* **382** 607
- [19] Fendler J H 2001 *Chem. Mater.* **13** 3196
- [20] Braun E, Eichen Y, Sivan U and Benyoseph G 1998 *Nature* **391** 775
- [21] Choi I S, Bowden N and Whitesides G M 1999 *Angew. Chem., Int. Edn Engl.* **38** 3078
- [22] Yang P D, Rizvi A H, Messer B, Chmelka B F, Whitesides G M and Stucky G D 2001 *Adv. Mater.* **13** 427
- [23] Petit C, Taleb A and Pileni M P 1998 *Adv. Mater.* **10** 259
- [24] Saado Y, Ji T, Golosovsky M, Davidov D, Avni Y and Frenkel A 2001 *Opt. Mater.* **17** 1
- [25] Jacobs H O and Whitesides G M 2001 *Science* **291** 1763
- [26] Jacobs H O, Campbell S A and Steward M G 2002 *Adv. Mater.* **14** 1553
- [27] Mesquida P and Stemmer A 2002 *Microelectron. Eng.* **61/62** 671
- [28] Krinke T J, Deppert K, Magnusson M H and Fissan H 2002 *Part. Part. Syst. Character.* **19** 321
- [29] Fudouzi H, Kobayashi M and Shinya N 2002 *Langmuir* **18** 7648
- [30] Wright W M D and Chetwynd D G 1998 *Nanotechnology* **9** 133
- [31] Jacobs H O and Stemmer A 1999 *Surf. Interface Anal.* **27** 361
- [32] Mesquida P and Stemmer A 2001 *Adv. Mater.* **13** 1395
- [33] Born A and Wiesendanger R 1999 *Appl. Phys. A* **68** 131
- [34] Krinke T J, Fissan H, Deppert K, Magnusson M H and Samuelson L 2001 *Appl. Phys. Lett.* **78** 3708
- [35] Mesquida P, Knapp H F and Stemmer A 2002 *Surf. Interface Anal.* **33** 159
- [36] Fudouzi H, Kobayashi M and Shinya N 2001 *Mater. Res. Soc. Symp. Proc.* **636** D9.8/1
- [37] Groff R, Khargonekar P, Koditschek D, Thieret T and Mestha L K 1999 *Proc. 38th IEEE Conf. on Decision and Control* vol 2
- [38] Pai D M and Springett B E 1993 *Rev. Mod. Phys.* **65** 163
- [39] Xia Y N and Whitesides G M 1998 *Annu. Rev. Mater. Sci.* **28** 153
- [40] Odom T W, Love J C, Wolfe D B, Paul K E and Whitesides G M 2002 *Langmuir* **18** 5314
- [41] Mazur K 1997 *J. Phys. D: Appl. Phys.* **30** 1383
- [42] Jacobs H O, Knapp H F, Muller S and Stemmer A 1997 *Ultramicroscopy* **69** 39
- [43] Jacobs H O, Leuchtman P, Homan O J and Stemmer A 1998 *J. Appl. Phys.* **84** 1168
- [44] Maximov I, Gustafsson A, Hansson H C, Samuelson L, Seifert W and Wiedensohler A 1993 *J. Vac. Sci. Technol. A* **11** 748
- [45] Jackson J D 1975 *Classical Electrodynamics* (New York: Wiley)
- [46] Schiel A, Weber A P, Kasper G and Schmid H-J 2002 *Part. Part. Syst. Character.* **19** 410
- [47] Chou S Y, Keimel C and Gu J 2002 *Nature* **417** 835